Ionics (2015) 21:1561–1575
DOI 10.1007/s11581-014-1336-4

ORIGINAL PAPER

Relaxation behavior in clay-reinforced polymer nanocomposites

A. L. Sharma · Awalendra K. Thakur

Received: 25 August 2014 / Revised: 10 November 2014 / Accepted: 27 November 2014 / Published online: 11 December 2014

Abstract The effect of clay reinforcement on dielectric, conductivity, and mechanical relaxation behavior of a polymer clay nanocomposite film is reported. Polymer nanocomposite is composed of three component polymers (polyacrylonitrile) as a host matrix, salt ($LiPF_6$) as conducting species, and clay (sodium montmorillonite) as intercalant. The macroscopic parameters like polymer glass transition temperature and available free mobile charge carriers have been analyzed properly using dynamic mechanical analysis and dielectric analysis. Dielectric analysis indicated distribution of relaxation time as a function of clay concentration, whereas conductivity spectrum exhibited dispersion at lower frequency followed by saturation region at intermediate frequency. The dispersion behavior is related to the electrode polarization attributed to faster ion dynamics. The dielectric and conductivity relaxation are in excellent correlation with mechanical relaxation owing to the changes in glass transition temperature due to polymer-ion-clay interaction. The proposed mechanism is a sequel to the experimental results.

Keywords Polymer nanocomposites · Mechanical relaxation · Dielectric analysis · AC conductivity renewable energy sources

A. L. Sharma · A. K. Thakur
Department of Physics and Meteorology, Indian Institute of Technology (IIT), Kharagpur 721302, India

A. K. Thakur
Department of Physics, Indian Institute of Technology (IIT), Patna 800013, India

A. L. Sharma (✉)
Centre for Physical and Mathematical Sciences, School of Basic and Applied Sciences, Central University of Punjab, Bathinda 151001, India
e-mail: alsharmaiitkgp@gmail.com

Introduction

Polymer nanocomposite materials have evoked extensive academic and industrial attention in the recent decade due to their unique properties [1–6]. Ion-conducting polymer nanocomposites (PNCs) have become increasingly important due to their potential applications in various electrochemical storage/conversion devices, such as high-energy-density lithium ion batteries, proton exchange membrane (PEM) fuel cells, and supercapacitors [6–10]. PNCs are a multicomponent system comprising polar polymer having solvating heteroatoms, alkali metal salt having bulky anion, and inert filler/clay as the adduct/dopant. Such a combination imparts structural disorder/amorphousity in the composite phase and it facilitates ion transport. The ion transport properties in PNC, in general, depend on wide-ranging factors, such as (i) structural phase and pathway for ion migration, (ii) sites available for mobility of charge carriers, (iii) rate of carrier mobility, (iv) cation (charge carrier) coordination pattern with the polymer chain, (v) polymer chain motion and its orientation, and (vi) flexibility of the polymer backbone structure. So, the ion dynamics and relaxation behavior in PNCs are strongly affected by the inner morphology as well as mechanical attributes of the polymer host on composite formation. In addition to the intrinsic variables, the response of the composite structure with extrinsic parameters like frequency and temperature is also important in determining the overall picture.

One very important aspect of electrical conduction in amorphous/disordered solid is the strong dispersion of electrical conductivity. At low frequency, it has been observed that the conductivity is independent of frequency. While at higher frequencies, conductivity is strongly dependent on frequency and it varies according to the Jonscher's universal power law [11–13]. This behavior appears to be a general feature in literature. We have also noted this feature in a few PNCs reported earlier by our group [14–17]. The results indicated

that all disordered PNCs show almost similar behavior so far as the frequency response of electrical conductivity is concerned. The most common explanation for strong dispersion in ac conductivity is the existence of one or the other type of inhomogeneities present in the material samples [18, 19]. However, an acceptable mechanism, consistent with the realities of the structural phase composition, physical structure of the host polymer, and pathway available for ion migration, is yet to emerge out. Our earlier works on a number of systems based on polymer such as solid polymer electrolytes (SPEs), composite polymer electrolytes (CPEs), and PNCs have demonstrated that ceramic dispersion and clay intercalation in the polymer salt complex increase ionic conductivity due to many factors, like changes in glass transition temperature, concentration of free charge carriers, and amorphous content in PNC matrix. However, the origin of dielectric polarization/relaxation and their correlation with mechanical properties has remained unexplored.

In this work, we report an elaborate discussion on the dielectric and mechanical properties of a polymer clay nanocomposite system based on $(PAN)_8LiPF_6+x$ wt% DMMT. The effect of organomodified clay concentration on dielectric (dispersion/relaxation) property of the ion-conducting PNC films has been analyzed and correlated with mechanical relaxation of the polymer host in the PNC. The large enhancement in mechanical and electrical conduction properties has been explained. A mechanism for stiffness in the PNCs, which is consistent with the dynamic mechanical analysis results, has been proposed.

Theoretical background

Dielectric analysis

The "dielectric" was coined by William Whewell in response to a request from Michael Faraday. Dielectric materials get polarized under the action of an external electric field. When dielectric materials are placed in an external electric field, the electrical charges are shifted from their equilibrium positions (positive charges are shifted along the electric field direction and negative charges are in the opposite direction). The term dielectric is typically used to describe materials with a high polarizability, which can also be expressed by a number called "dielectric constant."

In order to study the dielectric properties concerned, the storage and dissipation energy can be termed as permittivity of the materials. The permittivity can have real and imaginary component such that

$$\varepsilon* = \varepsilon' - j\varepsilon' \tag{1}$$

where ε^* is complex quantity of dielectric constant, ε' is the real value of dielectric constant which measures the storage ability of transport charge carriers, ε'' is the imaginary part of the dielectric constant which measures the loss of transport charge in prepared polymer nanocomposite films. The origin of dielectric permittivity in the conducting medium can be derived using the Maxwell's 4th equation (curl equation of magnetic field strength):

$$\left\{ \begin{array}{l} \Delta \times B = \mu_o J_{\text{enclosed}} + \mu_o \dfrac{\partial D}{\partial t} \text{ or} \\ \Delta \times H = J_{\text{enclosed}} + \dfrac{\partial D}{\partial t} = J_{\text{enclosed}} + j\omega D = \sigma E + j\omega\varepsilon_o\varepsilon' E = \omega\varepsilon_o\left(j\varepsilon' + \dfrac{\sigma}{\omega\varepsilon_o}\right)E' \end{array} \right\} \tag{2}$$

where $\varepsilon' = \frac{-Z''}{\omega C_o\left(Z'^2+Z''^2\right)}$ and $\varepsilon'' = \frac{Z'}{\omega C_o\left(Z'^2+Z''^2\right)}$

From the above equation, we can conclude that for a conducting medium (solid polymer electrolyte), the total dielectric loss mainly attributed to two contribution (a) loss due to permanent or induced dipole (ε") and (b) loss due to ionic conduction $\left(\frac{\sigma_{dc}}{\omega\varepsilon_o}\right)$. In the case of solid polymer electrolyte with appreciably high ionic conductivity, the dielectric relaxation due to dipole may thus be masked by the relaxation from polarization of the charged conducting species present in the material system [20, 21].

So the dielectric constants (ε' and ε'') giving the corresponding real and imaginary parts of conductivity obey the following relation $\sigma_1=\sigma_{ac}=\omega\varepsilon_o\varepsilon''$ and $\sigma_2=\omega\varepsilon_o\varepsilon'$, where ε_o is the permittivity in free space (8.85×10^{-14} F cm^{-1}). The imaginary part of dielectric permittivity is clearly related to real part of complex conductivity and vice versa. The real part of the complex conductivity is referred to as the ac conductivity (σ_{ac}). For a conducting medium, the ac conductivity may be defined as follows:

$$\sigma_{ac} = \omega\varepsilon_o\varepsilon'' = \omega\varepsilon_o\left(\frac{\sigma_{dc}}{\omega\varepsilon_o} + \varepsilon''_{(\text{corrected})}\right) \tag{3}$$

The first part of the ac conductivity is treated as the dc conductivity term, and the second term is varying with frequency (dispersive component) and at the same time varying according to Jonscher's power law ($A\ \omega^n$) in the limiting frequency range. The dielectric parameters (ε', ε'', σ_{ac}, and tan δ) are depended strongly on frequency, temperature, nature of electrical response, and interaction among charge carriers in the material sample. We have systematically analyzed this

interaction in the present studies. It is discussed in the "Results" section.

Mechanical analysis

The dynamic mechanical analysis (DMA), sometimes called dynamic mechanical spectroscopy, is a technique used to study and characterize the mechanical properties of the materials. It is most useful for studying the viscoelastic behavior of a polymer. A sinusoidal stress is applied and the strain in the material is measured, allowing one to determine the complex modulus. In dynamic mechanical spectroscopy, we are doing the measurement either in temperature or in frequency sweep leading to variations in the complex modulus. This approach can be used to find the glass transition temperature of the material, as well as to identify transitions corresponding to other molecular motions.

For a perfectly elastic solid, the resulting strain and the stress will be perfectly in phase; while in purely viscous fluid, there will be a 90° phase lag of the strain with respect to the stress. Viscoelastic polymers have the characteristics in between where some phase lag will occur during DMA tests. The mechanical modulus (Young's modulus) simply defines the ratio of the applied stress to the strain which is developed on materials.

$E = \frac{\sigma}{\varepsilon}$ where σ is the applied stress and ε is the produced strain on the sample materials. In order to obtain the exact relation among them, let us consider that a stress is applied across the sample

$$\begin{aligned} \sigma &= \sigma_o \sin(\omega t + \delta) \\ \sigma &= \sigma_o \sin\omega t \cos\delta + \sigma_o \cos\omega t \sin\delta \end{aligned} \tag{4}$$

and the generated strain will be $\varepsilon = \varepsilon_o \sin\omega t$, where modulus is the ratio of stress to strain so we can derive the value of mechanical storage and loss value from above equation as follows:

$$E* = E' \sin\omega t + E'' \cos\omega t \tag{5}$$

where $E' = \frac{\sigma_o}{\varepsilon_o}\cos\delta$ represents the storage part (real part) of the mechanical modulus and $E'' = \frac{\sigma_o}{\varepsilon_o}\sin\delta$ represents the loss part (imaginary part) of the mechanical modulus.

The components are related to complex modulus (E^*) as

$$E* = E' + jE'' = \frac{\sigma_o}{\varepsilon_o}(\sin\omega t + j\cos\omega t) \tag{6}$$

Here E' is the real part of the mechanical modulus corresponding to the mechanical storage part (elastic response to the deformation) of the materials; E'' is the imaginary part of the mechanical modulus corresponding to the mechanical loss part (plastic response to the deformation) of the materials. The ratio ($E''/E' = \tan\delta$) is useful for determining the occurrence of molecular mobility transitions such as the glass transition temperature. Both parameters (E' and E'') are strongly dependent on the frequency of applied force across the sample. We have systematically analyzed this molecular interaction in present studies. It is discussed in the "Results" section of mechanical analysis.

Experimental

Materials preparation

The PNC films were prepared via a standard solution cast technique, using polyacrylonitrile (PAN; Aldrich MW 1.5×10^5) as the host matrix and $LiPF_6$ (Aldrich) as the appropriate lithium salt. Nanocomposite formation was carried out using intercalation of polymer salt (PS) complex into nanometric clay channels of dodecyl-modified montmorillonite (DMMT) clay. The polymer host (PAN) and salt ($LiPF_6$) were vacuum dried at 120 °C for 32 h. An appropriate stoichiometric ratio of PAN was dissolved in *N*,*N*, dimethylformamide (DMF; Merck), and the solution was stirred for 18 h. Subsequently, a calculated amount (stoichiometric) of $LiPF_6$, was added into the PAN solution and stirred for 15 h to facilitate homogeneous mixing and complexation. The stoichiometric ratio of salt in the polymer host (PAN) matrix was maintained at an optimized ratio of $N/\mathrm{Li} = 8$. Next, DMMT clay was added into the polymer salt complex solution in different concentrations ($0 \le x \le 20$; where x refers to clay concentration with regards to PAN by wt) and stirred for 12 h. Finally, the composite solution was poured in polypropylene dishes and glass slide then allowed to dry under controlled conditions. Free-standing polymer nanocomposite films were obtained on solvent evaporation. So the series of PNC films obtained can be expressed as $(PAN)_8LiPF_6 + x$ wt% DMMT.

Materials characterization

Dielectric spectroscopy measurements of the nanocomposite films were carried out using a computer-interfaced impedance analyzer (HIOKI LCR Hi-Tester Model 3532, Japan) in the frequency range of 100 Hz to 1 MHz on a sample cell configuration of the type *SS* ‖ *PNC* ‖ *SS* (SS stands for stainless steel blocking electrodes and PNC for polymer nanocomposite films). An input ac signal of ~60 mV was applied across the cell to perform impedance measurement. Dynamic mechanical thermal analysis (DMTA) of the polymer nanocomposite films was performed on a DMTA Rheometric Scientific™ (model DMTA.IV), USA in tension-torsion mode. The experiments were carried out at constant frequency (1 Hz) at a heating rate of 2 °C min^{-1} with constant strain of 0.01 % over a temperature range of 30 °C to 120 °C. The storage modulus, E', loss modulus, E'', and loss tangent, tan δ, were measured for each sample in this temperature range. The samples (size 15 mm×10 mm×0.7 mm) were cut from the polymer nanocomposite films.

Results

The results related to the structural phase formation, morphology, Fourier transform infrared (FTIR) spectrum, electrical impedance analysis, etc. on $(PAN)_8LiPF_6+x$ wt% DMMT has been reported earlier [22] by us. It was noticed based on FTIR results that ion pairing is an important issue in such PNCs and it is very specific to the clay concentration. Further, the origin of dielectric properties in such a heterogeneous system may possibly be due to both to the electronic and ionic components. However, the true picture supported by experimental evidences remains to be examined. This has been investigated and explained as follows.

Dielectric spectrum analysis

Cole-Cole plot

KS Cole and RS Cole showed a feature of relaxation behavior with Cole-Cole diagram. The complex plane plot (Cole-Cole diagram) is used for the analysis of dielectric relaxation. In the Cole-Cole diagram, the loss factor ε'' is plotted against the real part of permittivity at a constant temperature and traces a semicircle, by which the time constant of dielectric relaxation can be determined using the expression $\omega\tau=1$. If the dielectric relaxation time (Debye-type relaxation) has a perfect semicircle, it is a clear feature that the materials have a single relaxation time. When as if often the case, the material composed of two or more than two constituents has a spread of relaxation times because of its heterogeneous construction. The diagram is a semicircular arc and not a standard semicircle. Cole and Cole showed that the relation between ε' and ε'' should also be a semicircle but the center of circle may lie below the ε' axis [23–26].

It is convenient to analyze the dielectric spectra in a complex plane. Figure 1 shows the Cole-Cole plot for the polymer nanocomposite films. In this plot when we move at a higher frequency, the data point moves from right side to left. The complex plane plot of ε' vs. ε'' shows the depressed semicircle whose center lies below the real axis. The complex plane plot fitted using the separate equations for real and imaginary part of the permittivity is given below:

$$\varepsilon' = \frac{\varepsilon_\infty + \Delta\varepsilon(1+\omega\tau)^\alpha \cos\left(\frac{\alpha\pi}{2}\right)}{1+2(\omega\tau)^\alpha \cos\left(\frac{\alpha\pi}{2}\right)+(\omega\tau)^{2\alpha}} \tag{7}$$

$$\varepsilon'' = \frac{\Delta\varepsilon(\omega\tau)^\alpha \sin\left(\frac{\alpha\pi}{2}\right)}{1+2(\omega\tau)^\alpha \cos\left(\frac{\alpha\pi}{2}\right)+(\omega\tau)^{2\alpha}}$$

where ε_∞, $_\Delta\varepsilon$, τ, and α are the permittivity at infinite, dielectric strength, relaxation time, and distribution (power law) exponent of the material sample, respectively. The real and imaginary parts of dielectric permittivity have been originated from the standard Cole-Cole relation $\varepsilon* = \varepsilon_\infty + \frac{\Delta\varepsilon}{1+(j\omega\tau)^\alpha}$ where notations have their usual meaning.

The fitted data are recorded in the Tables 1 and 2 at 30 and 100 °C respectively. From Table 1 we can say that on the increase of clay concentration, the exponent (α) goes on decreasing which is the clear indication of more distributed relaxation time. The relaxation time due to more than one charge carrier is of course present in the material system. The permittivity at infinity is increasing when adding the organoclay in the PS matrix. The value of ε_∞ is maximal at 7.5 wt% compared with other concentrated as well as clay-free PNC films. The other data (e.g., $_\Delta\varepsilon$ and C_p) are compared in the same table. (See Table 2).

Frequency response of real (ε′) and imaginary (ε″) permittivity

Figure 2a, b shows the variation of dielectric permittivity (ε') with frequency for PNC samples at room temperature (30 °C) and 100 °C (i.e., above polymer glass transition temperature (T_g)). The pattern of the real part of dielectric permittivity (ε') variation indicates two distinct regions of changes (marked as regions I and II in Fig. 2a, b), irrespective of organoclay concentration. Region I exhibits strong frequency dependence (highly dispersive region) followed by region II where ε' seems to be almost constant with the frequency irrespective of the clay composition both at room temperature and 100 °C. The high value of dielectric permittivity (ε') observed in the low-frequency region (region I) is attributed to the accumulation of space charge [27] near the electrode-electrolyte interface due to the polarization effect. The overall effect causes immobilization of charge carriers at low frequency by which the value of dielectric permittivity became so high. The real part of dielectric permittivity (ε') decreases on increase of frequency due to high periodic reversal of the field at the interface. With increasing frequency, a consequent reduction of charge carriers occurs that contributes in lowering the dielectric constant. In region II, the lowering of the real part of permittivity may be due to the weakening of ion-ion interaction in the transient dipoles [28] (lithium to electron-rich site of the polymer) i.e., in the dc conduction. The overall effect would be the migration of charge carrier due to long-range ion transport. The almost constant region (region II) appears to be very interesting when we have plotted the data in the limited frequency range (0.5 to 6 MHz) at room temperature and at 100 °C which are embedded in the inset of its room temperature and 100 °C (Fig. 2a, b). It has been observed from the inset of Fig. 2a that the dielectric permittivity increases on adding the organoclay in PS matrix. The nature of the variation of dielectric constant (ε') is almost the same at room temperature and at 100 °C. However, the enhancement is clearly visible in the latter case. This may be due to the flexibility of the polymer chain in the PNC matrix.

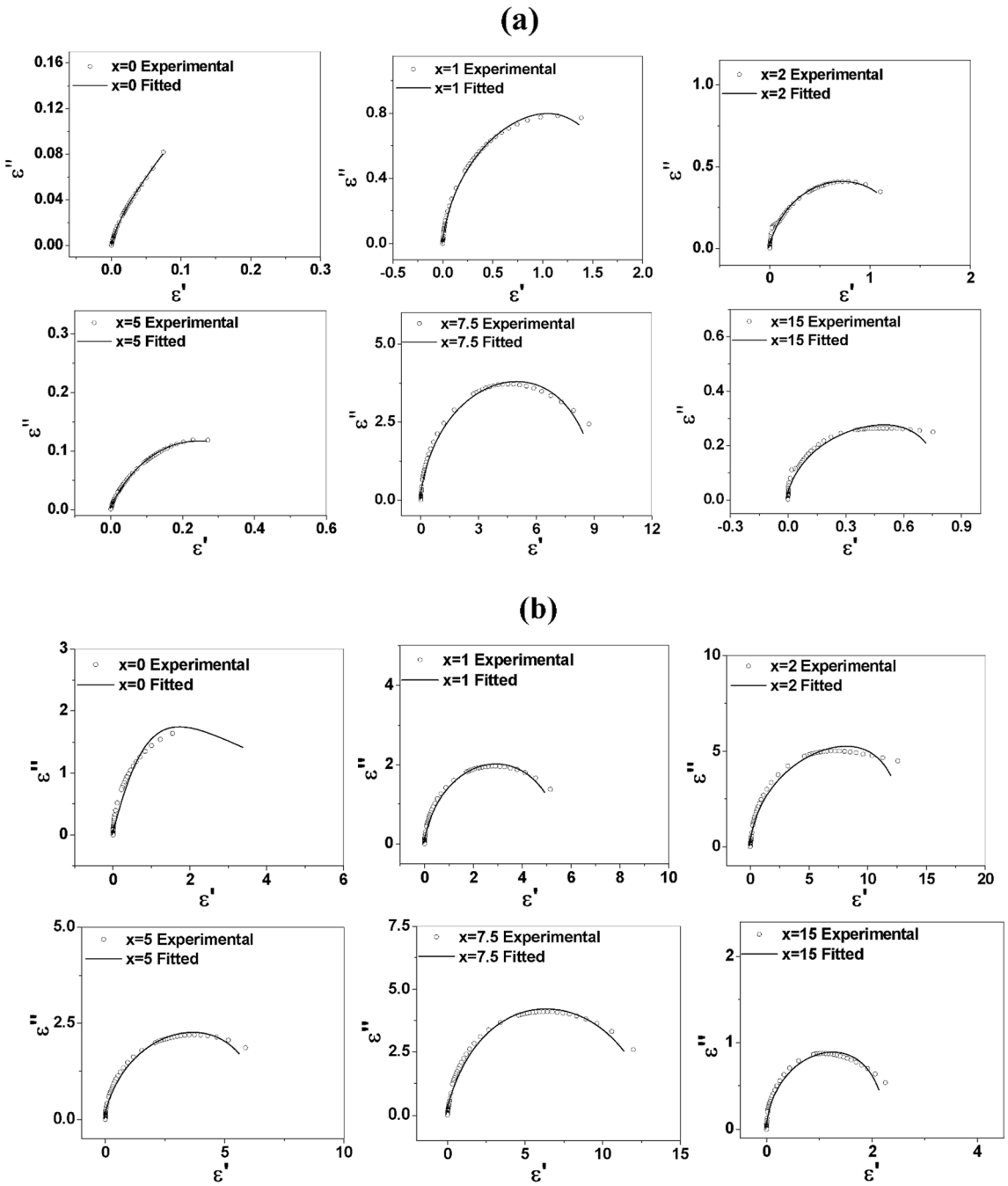

Fig. 1 **a** Cole-Cole plot of polymer nanocomposite films at room temperature based on $(PAN)_8LiPF_6$+*x* wt% DMMT. **b** Cole-Cole plot of polymer nanocomposite films at 100 °C based on $(PAN)_8LiPF_6$+*x* wt% DMMT

Figure 3a, b indicates the variation of the imaginary part of dielectric permittivity (total dielectric loss) vs. frequency at room temperature and 100 °C, respectively. The magnitude of dielectric strength is increased drastically on immediate addition of organoclay in the PS matrix. The value of dielectric strength has been increased drastically at certain critical concentration (say ~7.5 wt%). The enhancement of dielectric strength has been observed at 100 °C when compared with the room temperature dielectric (ε') result. The imaginary component of the dielectric permittivity (dielectric loss) originated due to the contribution of energy absorbed by the dipoles (relaxing, ionic, permanent, etc.) present in the material system. However, an ionic conductor bulk conductivity of the polymer electrolyte also plays an important role. In the case of polymer electrolytes, the high dc conductivity normally suppresses the loss contributed by the dipoles present in the material system. In order to estimate the actual dipolar contribution, it is necessary to subtract dc contribution from the total dielectric loss. The corrected dielectric permittivity ($\varepsilon''_{\text{corrected}}$) obtained after subtracting the dc conductivity contribution ($\frac{\sigma_{dc}}{\omega\varepsilon_o}$) from the

Table 1 The fitted dielectric parameters (ε_∞, ε_s, C_p, α) at 30 °C

Clay concentration (%)	ε_∞	ε_s	C_p(nF)	α
0	84	74,951	19	0.83
1	125	1,386,729	1.4	0.81
2	284	1,103,794	1.5	0.69
5	308	1,270,786	8.9	0.59
7.5	752	8,740,670	7.8	0.86
10	426	1,843,281	8.6	0.74
15	545	752,432	1.2	0.73
20	352	238,075	1.7	0.74

observed (ε''_{total}) dielectric permittivity is expressed as

$$\varepsilon''_{corr} = \varepsilon''_{d} = \frac{Z'}{\omega C_o\left(Z'^2 + Z''^2\right)} - \frac{\sigma_{dc}}{\omega\varepsilon_o} \tag{8}$$

This equation gives a clear picture of the presence/absence of dipolar relaxation in a material system. The variation of imaginary part of corrected dielectric permittivity ($\varepsilon''_{corrected}$) vs. frequency at room temperature and at 100 °C is shown in the Fig. 3c, d. A comparison indicates that the $\varepsilon''_{corrected}$ peak has a lower value than ε''_{total}. The presence of the relaxation peak is always at a higher frequency in PNC samples when compared with clay-free PS complex film sample. The lowering of relaxation times observed by Fig. 3c, d in PNC samples when compared with PS complex is a clear indication of faster ion conduction.

Frequency response to dielectric loss

The loss tangent of the sample can be obtained from above-derived equation and may be defined as the ratio of the lossy reaction to loss less reaction in the Maxwell IV equation for conducting media defined as

$$\tan\delta = \frac{\left(\frac{\sigma_{dc}}{\omega\varepsilon_o} + \varepsilon''_{corrected}\right)}{(\varepsilon')} \tag{9}$$

Table 2 The fitted dielectric parameters (ε_∞, ε_s, C_p, α) at 100 °C

Clay concentration (%)	ε_∞	ε_s	C_p (nF)	α
0	51	547,126	0.32	0.82
1	164	5,152,231	0.16	0.80
2	200	12,556,094	0.58	0.81
5	174	5,876,540	0.21	0.76
7.5	482	2,594,300	0.17	0.76
10	412	12,724,446	0.54	0.80
15	89	3,000,000	0.23	0.82
20	88	2,728,077	0.56	0.82

Figure 4a, b compares loss tangent (tan δ) of the polymer nanocomposite films where the range of organomodified clay concentration varies $0 \le x \le 20$. It is well known that the dielectric loss is dependent on the number of parameters like absorption, frequency resonance, and charge-conducting species. In fast ionic conductors, generally, materials behave as lossy which are very much harmful for energy storage devices. In this dielectric loss pattern (tan δ vs. frequency), it has been observed that the relaxation peak observed at 59 kHz is shifted towards the higher frequency side just after the addition of organomodified montmorillonite clay into the polymer salt complex matrix. The peak shifting towards higher frequency has also been observed at 100 °C when compared with room temperature relaxation (Fig. 4b). The frequency observed at higher temperature (100 °C) is 346 kHz. The lowering of relaxation time irrespective of clay concentration and temperature is the clear indication of faster ion dynamics.

Conductivity spectrum

The ac conductivity of all samples ($0 \le x \le 20$) has been calculated using Eq. 3. Figure 5a shows a typical plot of the conductivity spectrum (i.e., ac conductivity vs. frequency) of polymer nanocomposite films with different clay concentrations (say, x=0, 1, 2, 5, 7.5, 10, 15, and 20) at room temperature. The representative ac conductivity plot of PS complex sample at room temperature and 100 °C is shown in the inset of Fig. 5a. The inset figure of the PS sample at room temperature clearly indicates that there are three distinct regions attributed by three different phenomena present in the material system. The lower-frequency dispersive region gives the sign of electrode polarization present in the material system. The constant region exhibits the long-range conduction of charged carriers in the material sample at intermediate-frequency range. The region III i.e., high-frequency dispersive region is due to the hopping of charge carriers (to-and-fro motion) at higher-frequency side. The ac conductivity variation with the frequency of PS sample is almost identical at 100 °C, except the dispersive point (characteristic frequency or hopping frequency) on the frequency axis which is shown in the same inset figure. It has been observed that at 100 °C the dispersive point is shifted towards higher frequency when compared with the same sample at room temperature. The frequency dependence of the conductivity is a typical behavior of ionic conductors. The frequency-independent conductivity is called the bulk/dc conductivity (σ_{dc}). The electrical conductivity increment at high-frequency region for PS sample at room temperature and 100 °C has been fitted through the Jonscher's universal power law [29]:

$$\sigma_{ac} = \sigma_{dc} + A\omega^n \tag{10}$$

where σ_{dc} is the dc conductivity, A is a prefactor having weak dependence on temperature, ω is the angular frequency and n

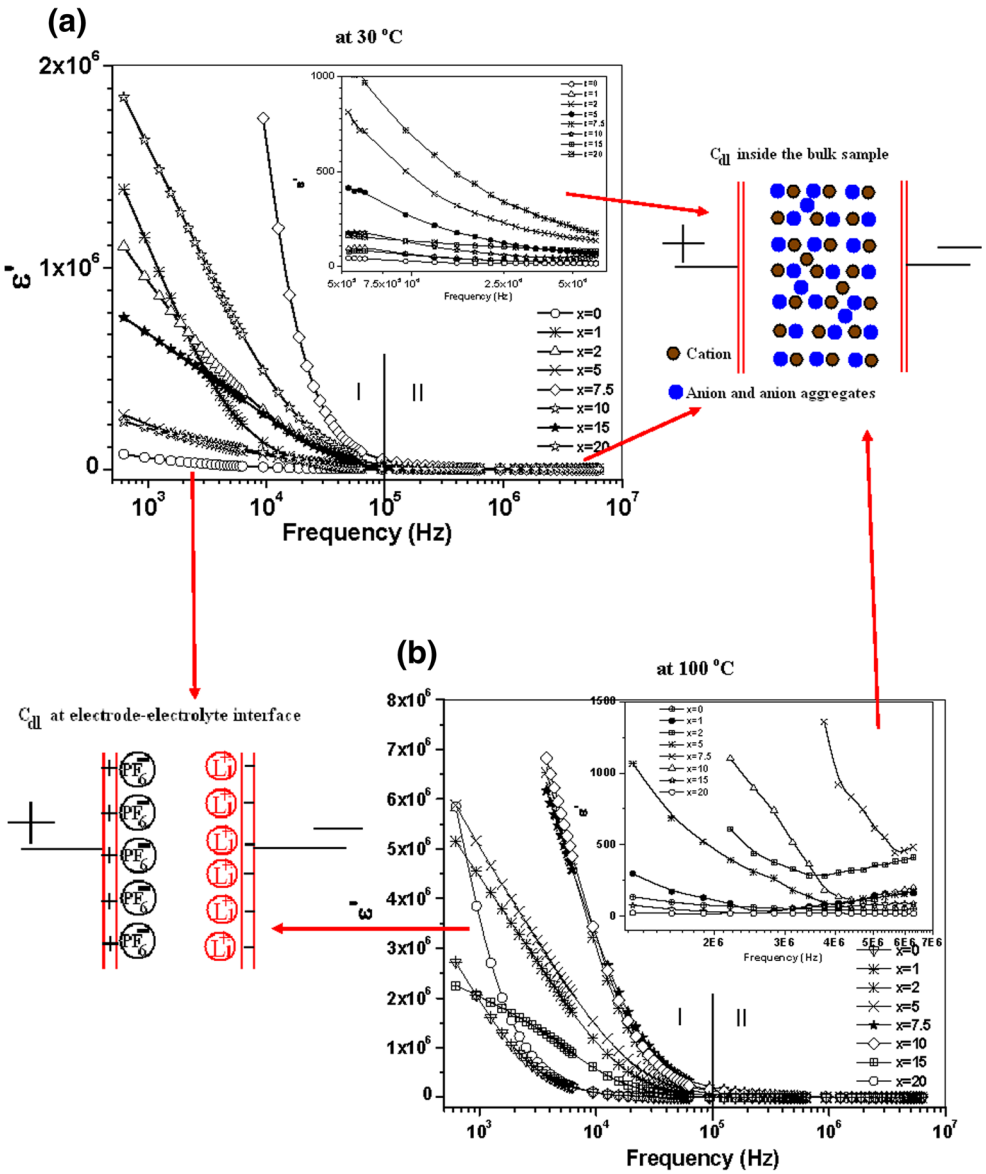

Fig. 2 The variation of real part of permittivity vs. frequency (**a**) at room temperature (**b**) at 100 °C

is the temperature-dependent power law exponents with $0<n<1$, which decreases on increasing the temperature. Also at a given temperature, the hopping frequency can be identified as the frequency at which ac conductivity becomes two times of dc conductivity expressed as

$$\left\{\begin{array}{l}\sigma_{ac}=\sigma_{dc}+A\omega^{n}\\ \sigma_{ac}=\sigma_{dc}\left(1+\left(\frac{\omega}{\omega_{P}}\right)^{n}\right)\\ \sigma_{ac}=2\sigma_{dc}\quad \text{when } \omega=\omega_{P}\end{array}\right\} \tag{11}$$

The frequency-dependent ac conductivity of the PS complex sample at room temperature and at 100 °C is well fitted with the Jonscher's universal power law. The critical exponents are estimated in the inset of Fig. 5a. The frequency dependence of the electrical conductivity starts at a critical frequency referred to as the characteristic frequency (ω_h) that was observed in the polymer salt complex film at room temperature and at 100 °C. From the fitting of universal Jonscher's power law, the estimated value of the critical frequency (ω_h) is ~95 kHz at an ambient temperature whereas for 100 °C, the value goes on the higher side at 942 kHz.

In this experimental observation of Fig. 5a, it has been observed that the lower frequency side exhibits the electrode-electrolyte interface region where the charge carriers get blocked and the conductivity became smaller. A comparison indicates substantial conductivity enhancement for PNC sample when compared with PS sample. The dc conductivity comes because of short-range pair-wise motion at the adjacent site of the heterosite of polymer, whereas on increasing the frequency beyond the hopping, the charge carriers are not getting sufficient time to reach the next available hopping site which results to back-and-fro motion and ac conductivity increases according to universal Jonscher power law. The

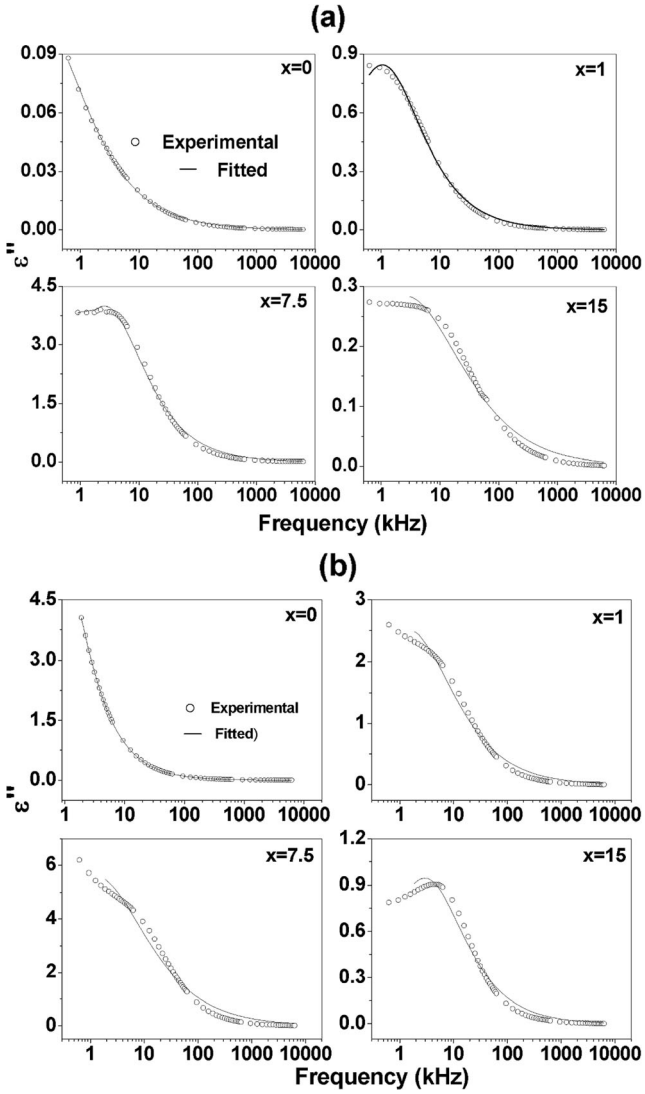

Fig. 3 The variation of imaginary part of permittivity with frequency (**a**) at 30 °C (**b**) at 100 °C, the variation of imaginary part of corrected permittivity with frequency (**c**) at 30 °C (**d**) at 100 °C

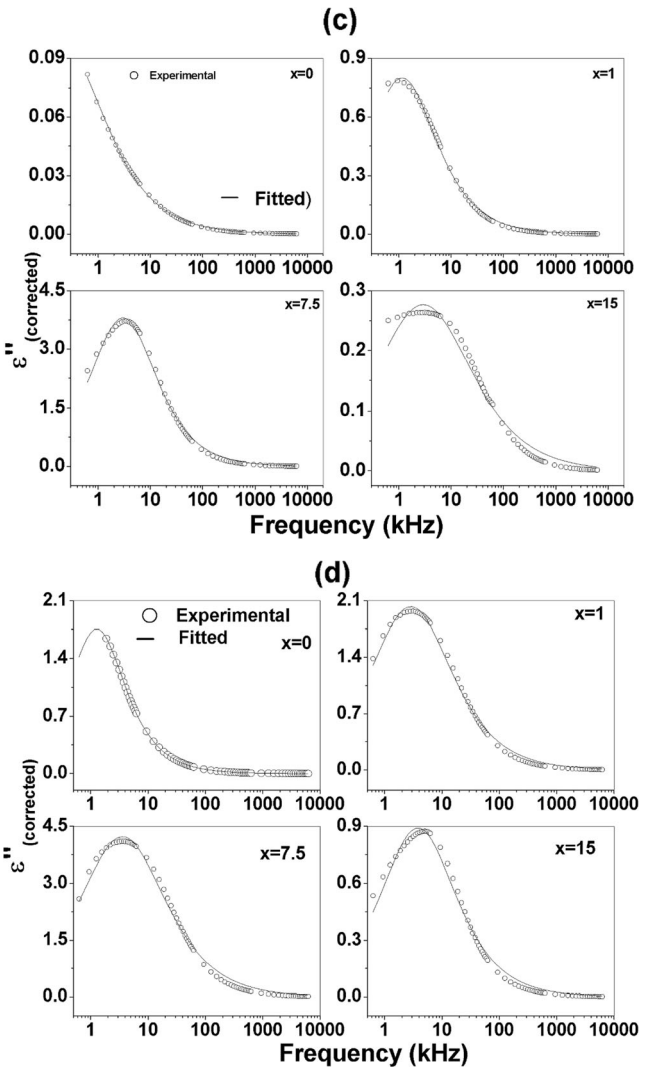

Fig. 3 (continued)

characteristic frequency (ω_h) shows the response of the material when it starts the frequency-dependent conductivity. This shifts towards the higher-frequency side after increasing the clay concentration. This may be because of the release of more free charge carriers after adding the organomodified montmorillonite clay in polymer salt complex sample. On increasing temperature, the dissociation will increase which favors the increase of the number of free charge carriers. At low frequency, an ion jumps from one site to its neighboring vacant site successfully contributing to dc conductivity. Figure 5a shows that there are three regions, but region III is suppressed due to the high dc conduction and limitation of impedance analyzer. To see the third region clearly in Fig. 5a, we have plotted the conductivity data in the limiting frequency range (0.5 to 7.5 MHz) in the Fig. 5b. With the help of Fig. 5b, we can say that all clay-concentrated PNC films obey the universal Jonscher's power law. Jonscher's fitting cannot be done because of the limiting data point, but we can say that the critical frequency (ω_h) shifted towards the higher-frequency side on immediate addition of organoclay in the PS complex matrix. The dc conductivity estimated from ac conductivity vs. frequency results best matches with the bulk conductivity obtained from the complex impedance spectrum of Nyquist plot.

Dynamic mechanical analysis

The DMA of $(PAN)_8LiPF_6$+x wt% DMMT-based PNC films has been studied to analyze their mechanical response under the action of thermally driven mechanical force. DMA measures the response of a given material to a cyclic deformation as a function of the temperature. Figure 6a shows the variation of mechanical storage modulus with respect to temperature under the action of thermally driven mechanical force for different modified clay concentrations (x wt%). It has been noticed in Fig. 6a that the mechanical storage modulus

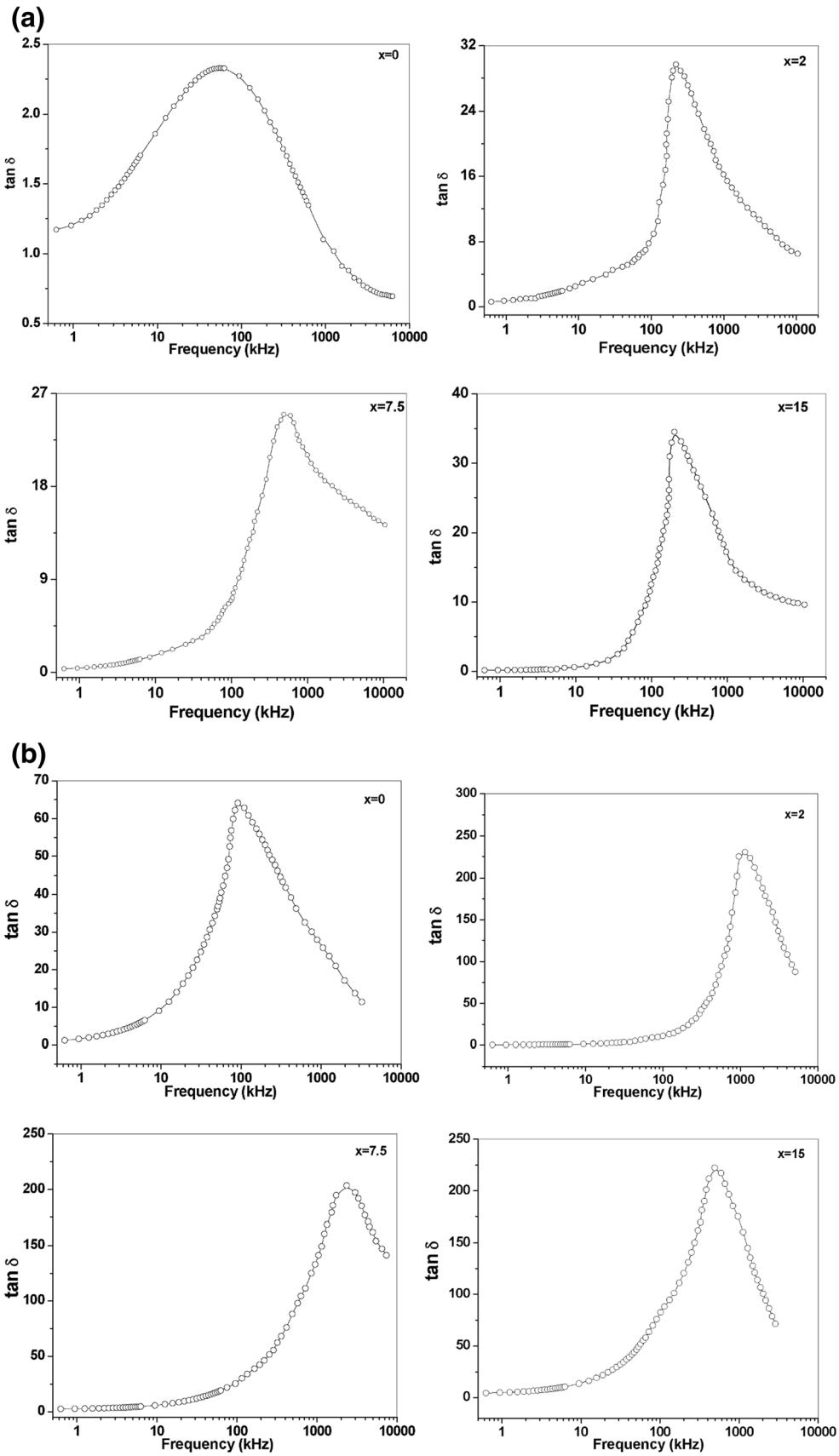

Fig. 4 **a** The loss spectrum of polymer nanocomposite films at 30 °C. **b** The loss spectrum of polymer nanocomposite films at 100 °C

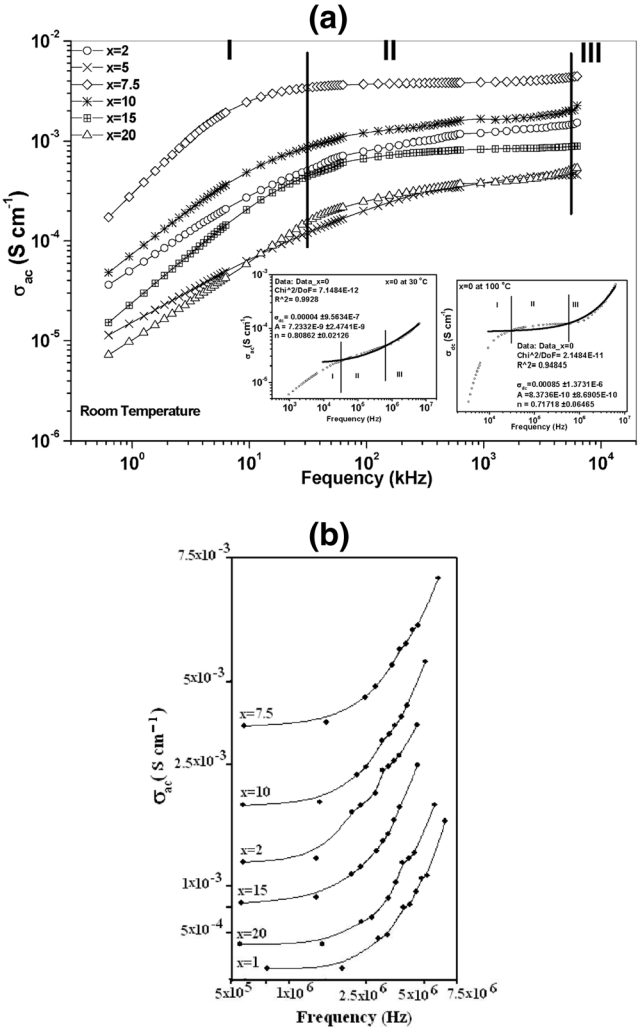

Fig. 5 The ac conductivity spectrum of PNC films **a** at room temperature and **b** in a selected frequency region

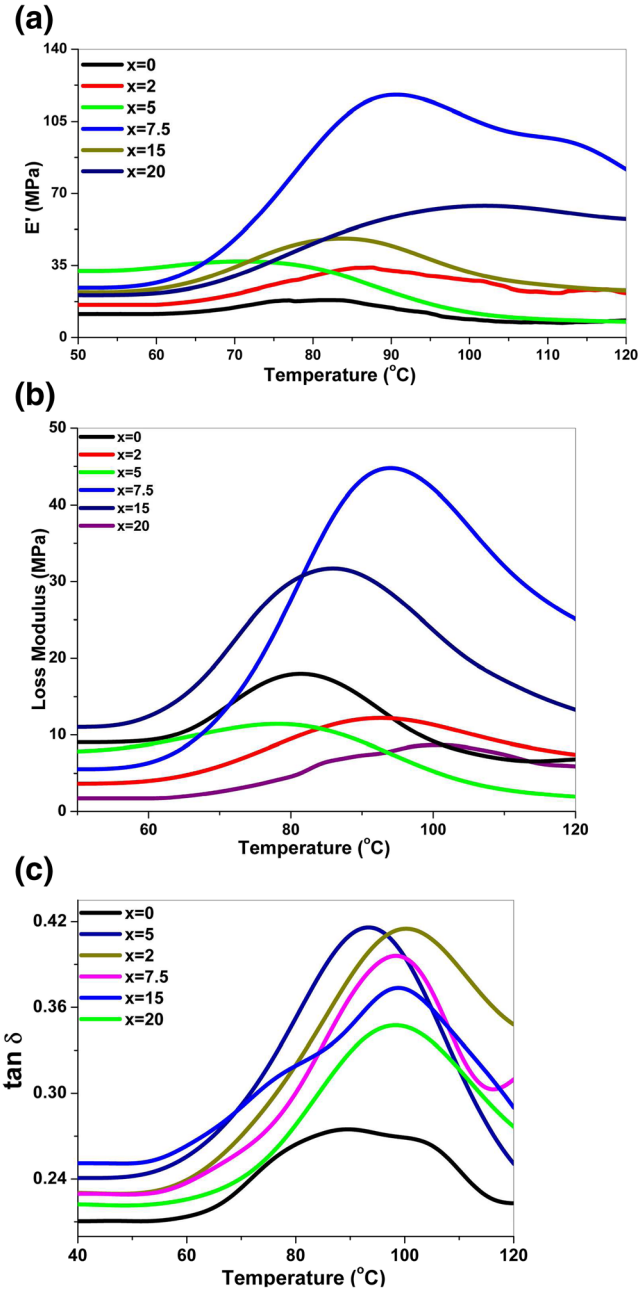

Fig. 6 **a** Plot of dynamic storage modulus vs. temperature of polymer nanocomposite films. **b** Temperature dependence mechanical loss modulus of polymer nanocomposite films. **c** Loss pattern of tan δ vs. temperature of polymer nanocomposite films. **d** Deconvoluted pattern of tan δ vs. temperature of polymer nanocomposite films based on $(PAN)_8LiPF_6$+*x* wt% DMMT

increases up to a certain temperature beyond which it decreases and finally becomes constant.

This type of signature has been observed for all clay-loaded polymer nanocomposite films. The nature of variation of mechanical storage modulus up to the glass transition temperature is may be due to the transient crosslinking of the cation to the side chain (heterosite) of the host polymer; while in the case of clay-based polymer nanocomposite films, the variation of mechanical storage modulus with temperature could be attributed to the electronegativity of the dipole present in the organomodified montmorillonite clay. A remarkable improvement in E' could be an outcome of the strong interaction between the PS complex and dipolar clay. In spite of the clay content, E' increases with increasing temperature and a transition can be seen at about ~70–90 °C. It seems that E' retains its strength over a wide temperature range on addition of the clay in the PNC phase. This may be due to the effect of imposing clay restriction on the molecular motions of the host polymer in polymer nanocomposite sample. The storage modulus of all PNC films is relatively higher over the entire temperature range when compared with that of the clay-free PS complex film. The increase of the mechanical moduli at 50 °C for all PNC films is 38, 178, 108, 91, and 79 % for *x*=2, 5, 7.5, 15, and 20 wt% modified clay concentration, respectively, when compared with the polymer salt complex film. On the other hand, moduli at the glass transition temperature

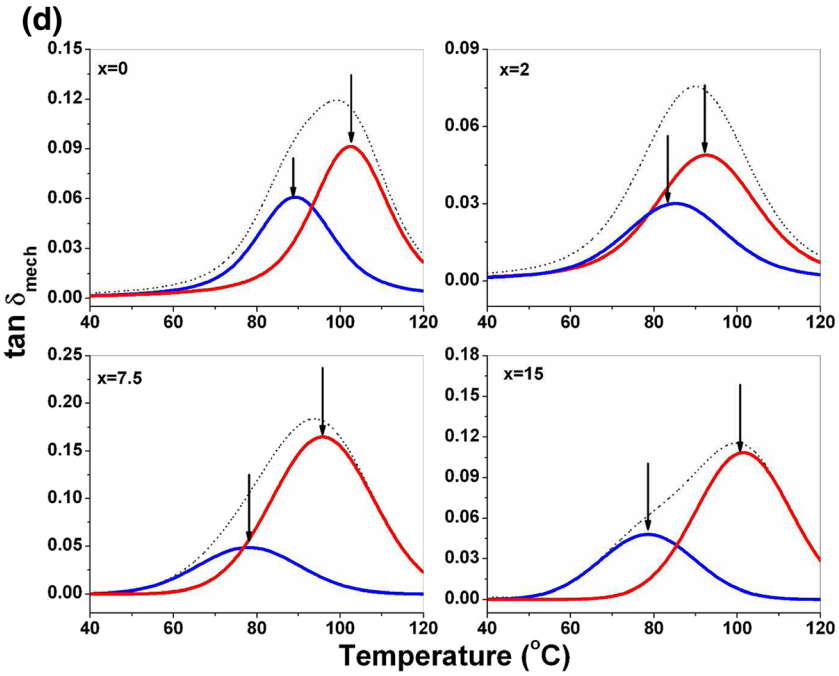

Fig. 6 (continued)

are recorded to be 83, 89, 405, 161, and 166 % for x=2, 5, 7.5, 15, and 20 wt% modified clay-concentrated PNC films when compared to that of the PS complex (Fig. 6a). The nature of variation of the mechanical storage modulus seems to be constant on and above 110 °C. Furthermore, at the temperature range of 40–120 °C, all the nanocomposite films exhibit much higher enhancement of E' as compared to that of neat PS complex. The enhancement of the mechanical storage of the polymer composite films keeps on increasing with respect to the organomodified clay concentration up to a certain clay concentration. On the basis of X-ray diffraction [22] in intercalated-type polymer nanocomposite films, the polymer films have a strong support. Moreover, at a large clay concentration, the mechanical storage value increases but affects the conducting phenomena of the materials. This may be due to the mechanical reinforcement effect of organomodified montmorillonite clay on the polymer salt complex film. The storage modulus becomes constant after certain temperature, providing a signature of mechanical equilibrium beyond the phase transition from glassy to rubbery phase of the host polymer.

Figure 6b shows the variation of mechanical loss vs. temperature (40 to 120 °C) at different organomodified clay concentrations. The lost part of the mechanical modulus increases up to glass transition temperature. Beyond this temperature, the mechanical loss of the polymer nanocomposite film samples decreases. This could be due to the transformation of materials from glassy to rubbery phase. It has also been observed that on increasing temperature, the natural frequency of the material system changes. The glass transition temperature best exhibits equilibrium with the applied driven mechanical force frequency. Beyond that, there may be frequency mismatch causing lowering of the mechanical loss. On the other hand, up to T_g, the enhancement of E'' is significant in the intercalated PNC films unlike that of E'. This behavior has been ascribed to the preferential segmental motion at the organic-inorganic interface neighborhood in the intercalated polymer nanocomposite films.

Figure 6c shows the variation of mechanical loss tangent vs. temperature at different organomodified clay concentration. The variation shows that the mechanical loss tangent is maximal at the glass transition temperature of the polymer nanocomposite films. At T_g, there is a substantial drop in E' with a peak in tan δ indicating viscous damping due to the segmental motion in the polymer. It may be related to the hindered molecular motions of the polymer chains caused by clay interaction. It is corroborated by a sudden decrease in T_g with increasing organomodified clay concentration when compared with pure polymer salt complex. This may be attributed, without any ambiguity, to the polymer-clay interactions. Such a possibility has already been observed in the FTIR results [30] and is corroborated by the reinforcement of the height of the tan δ peaks with increasing clay concentration in the DMA response.

The peaks in the Fig. 6c correspond to the T_g of the host polymer which undergoes a shift with varying clay loading in the PNC films. Some reports suggest these results in the suppression of glass transition due to the presence of the clay [31, 32]. The maximum shift in T_g as measured in the present result is ~10–20 °C. It is believed that the chemical bonding at the interface of the silicate and polymer salt matrix could lead to hindered relaxational mobility in the polymer segments near the interface, causing broadening and decreasing of T_g

[33–40]. Under the action of thermally driven mechanical energy, the PNC system is capable of withstanding and stores energy up to ~100 °C. In the rubbery state at temperatures above T_g, the molecular mobility of the polymer is much higher than in the glassy state.

Figure 6d shows the deconvoluted pattern of mechanical loss tangent (tan δ vs. temperature) of the PNC films. The peak asymmetry (Fig. 6c) prompted us to use Voigt profile fitting of the temperature evolution of mechanical loss pattern. It gave two distinct contributions in the tan δ vs. temperature profile. The deconvoluted mechanical loss peak occurring at lower temperature is attributed to the glass transition temperature of the PS complex, whereas the high-temperature loss peak could be related to the glass transition temperature of the host polymer (PAN). The glass transition temperature peaks in the DMA loss pattern basically refers to the structural phase transition from a rigid framework structure (plastic phase) to an elastomeric (rubbery) phase under thermomechanical stress. This estimate for T_g is therefore considered relatively reliable than that obtained from DSC. Results indicate that a lowering in the glass transition (T_g) temperature occurs at lower clay concentration when compared with respect to that of the PS complex. A relative lowering in T_g at lower clay-loading points is towards the enhancement in the flexibility of the polymer backbone. This in turn may be expected to increase the polymer chain motion in the PNC phase. Since cation coordination occurs at electron-rich site (−C≡*N*) of the host polymer, any enhancement in the polymer chain motion basically favors faster ion dynamics.

Such an effect, therefore, may cause substantial tailoring of electrical conductivity of the PNC films depending on the fraction of clay loading. This has, in fact, been observed in the electrical properties results. The mechanism related to this phenomenon is proposed to be discussed below in a mechanism.

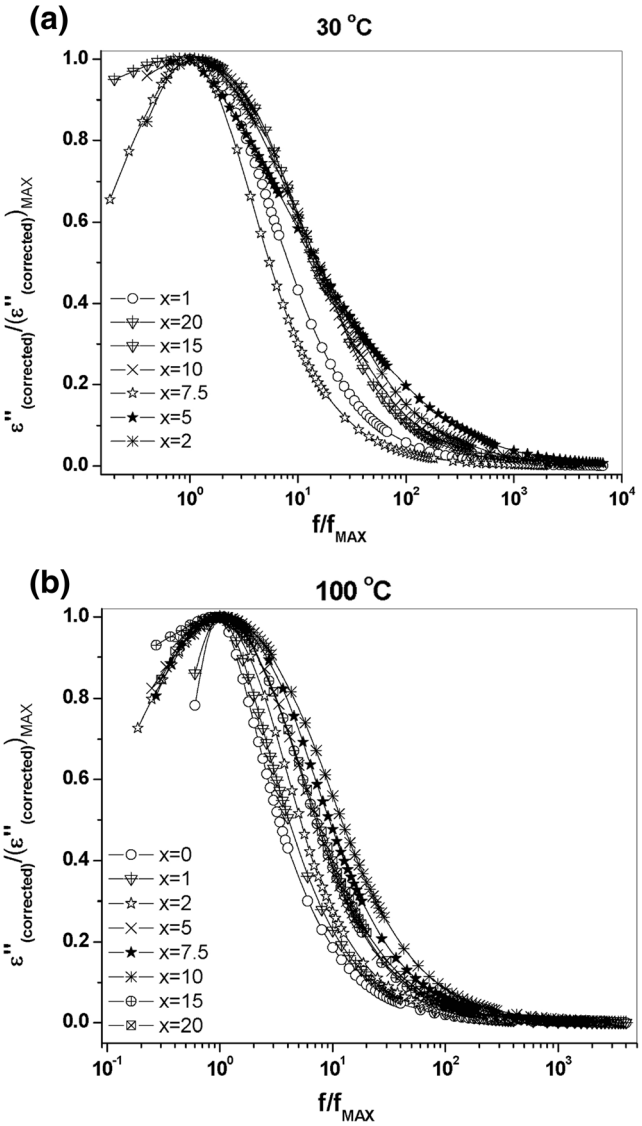

Fig. 7 Scaling behavior of permittivity in PNC films at **a** room temperature and **b** 100 °C

Discussion

Scaling behavior of permittivity spectra

Figure 7a, b shows the master curve permittivity ($\varepsilon''_{corrected}$) spectrum. In this spectrum, the frequency axis is normalized by f_{max} (frequency corresponding to $(\varepsilon''_{corrected})_{max}$) and that of $\varepsilon''_{corrected}$ by $(\varepsilon''_{corrected})_{max}$. From Fig. 7, it is clear that all the plots at different organoclay concentrations are overlapping at the start and end points, but it indicates that they are not overlapping in the whole range in a single master curve. It is a clear indication that the dynamical process occurring in our material samples at different frequencies does not have the same relaxation mechanism [41].

Correlation of dc conductivity with relaxation time (τ_ε and $\tau_{\tan\,\delta}$)

The variation of dielectric constants with frequency has generally been called dielectric relaxation spectroscopy (DRS). DRS is observed due to the number of different polarization mechanisms. The presence of any dielectric relaxation corresponds to one or more possible polarization mechanisms that occur on a microscopic level. Each relaxation process describes the decay of its polarization with time in a periodic field [42].

The dc conductivity has been estimated using the complex impedance plot. The CIS plot shows the semicircle at the higher-frequency region followed by a spike at the lower frequency. The intercept of semicircle on the real axis is the real estimation of the bulk resistance of the material samples.

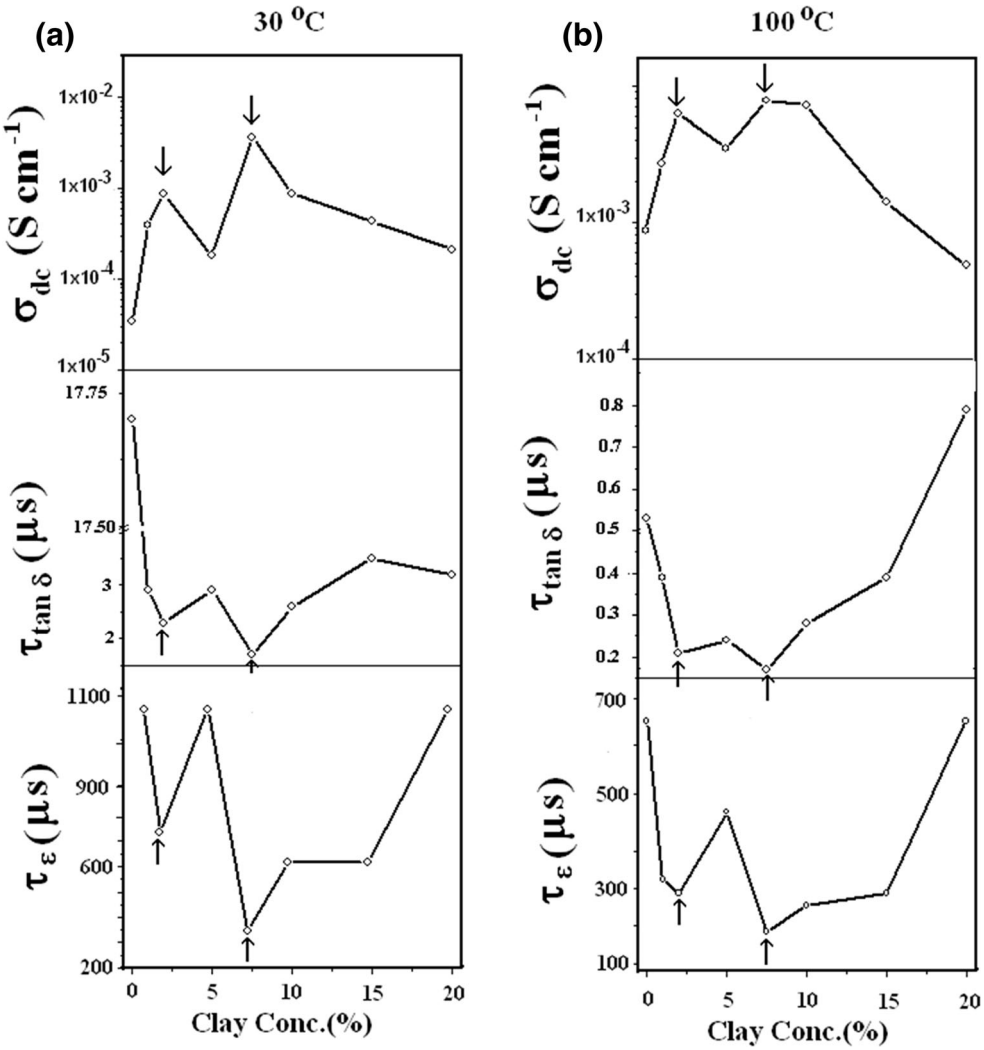

Fig. 8 The dc conductivity correlation with relaxation time at **a** 30 °C and **b** 100 °C

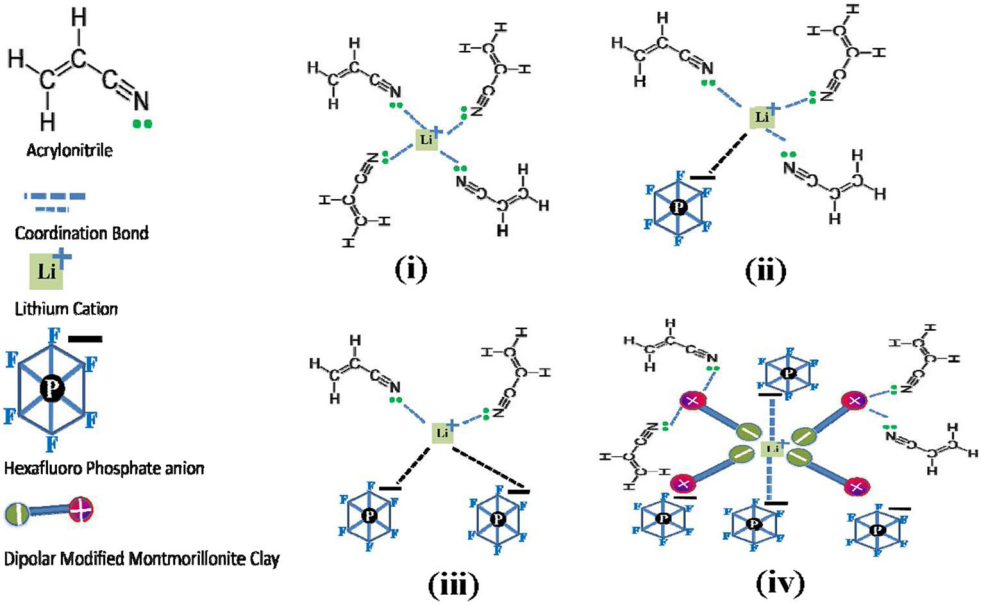

Fig. 9 Representation of transient cross-linking of polymer segments (*i*) direct cation coordination, (*ii*) via cation-anion interaction, (*iii*) both by cation and cation-anion with polymer interaction, and (*iv*) filler-polymer interaction by cation-anion interaction

Now the dc conductivity has been estimated using the widely known relation $\sigma_{dc} = \frac{1}{R_b}\left(\frac{\ell}{A}\right)$, where the conductivity is inversely proportional to the relaxation time (τ) which is given as $\sigma_{dc} = \frac{1}{R_b}\left(\frac{\varepsilon_o}{C_o}\right) = \frac{\varepsilon_s{}^2\varepsilon_o}{\Delta\varepsilon.\tau}$ where $\Delta\varepsilon$, ε_s, ε_o, and τ are dielectric strength, static permittivity, permittivity in free space, and relaxation time, respectively [41, 43]. It is mentioned clearly that although τ could not be measured for PS complex at room temperature, the effect is noted in the addition of organoclay PS complex matrix. A best correlation has been built in the dc conductivity and the relaxation time (τ_ε and $\tau_{\tan\,\delta}$) (Fig. 8a, b) obtained from dielectric spectrum. It is necessary to mention here that the relaxation time estimated from imaginary part of permittivity is much higher than the relaxation time obtained from tan δ which is well obeying the previously reported literature [42, 44].

Mechanism

It is believed that Li^+ may coordinate with a maximum of five electron-rich sites of the host polymer [45, 46]. In polymer salt complexation, ion-polymer interaction leads to the formation of inter- or intra-molecular transient crosslinking [47–49]. This limits the flexibility of the host polymer backbone matrix, resulting in a stiff matrix of the material sample. There are three types of possibility for transient crosslinking: (i) transient crosslinking directly through cations, (ii) transient crosslinking through cation-anion interaction, and (iii) transient crosslinking through both. In view of this, a possibility of transient crosslinking of polymer backbone via Li^+ coordination may be the likely feasibility. The feasibility scheme has been presented in the Fig. 9. It has been observed that the addition of nanometric organomodified montmorillonite clay affects the material sample in terms of stiffening of the polymer segments. The nanometric organoclay may show a net dipolar shift in the dielectric medium-like polymer salt complex matrix. The electropositive end of organoclay may interact with either electronegative end of the heterosite of the host polymer or with bulky anion present in the PNC matrix. The other end (electronegative) of the organoclay dipole will affect the other segment of the host polymer/free charge cation present in the sample matrix as illustrated in Fig. 9 (iv). The strong interaction of organoclay with host polymer has already been observed in the FTIR and dielectric results [42] of PNC films with different clay loading. As a result, PNC matrix polymer backbone gets strengthened due to the stiffening of the polymeric segments (chain) on nanometric clay addition which causes natural enhancement in the mechanical strength of the PNC films.

Conclusions

Intercalated PNC films based on $(PAN)_8LiPF_6 + x$ wt% DMMT has been prepared using standard solution cast technique. Dielectric and mechanical spectroscopy analyses have been done in the present study. In dielectric analysis, we have determined the dielectric properties of PNC films on ion dynamics in the heterogeneous composite phase. The electrical conductivity is improved drastically in the addition of organomodified clay in polymer salt complex film. Jonscher's power law fitting shows three regions (ac conductivity vs. frequency): low-frequency dispersion region, intermediate saturation, followed by high-frequency dispersion region. DRS is observed due to the number of different polarization mechanisms. The optimized combination of the PNC film may be expected to serve the dual purpose of electrolyte as well as separator in energy storage device, such as lithium polymer batteries and supercapacitors.

References

1. Amendola E, Scamardella AM, Callegaro G, Lavorgna M, Piscitelli F, Romeo V (2012) Epoxy nanocomposites based on silylated montmorillonite: effect of the coupling agents structure on the mechanical properties. Open Macromolec J 6:33–36
2. Pandey GP, Agrawal RC, Hashmi SA (2009) Magnesium ion-conducting gel polymer electrolytes dispersed with nanosized magnesium oxide. J Power Sources 190:563–572
3. Yuan Q, Challa VSA, Misra RDK (2014) Nanoscale elastic–plastic deformation in clay-reinforced nanostructured materials: the response of phase and structural morphology. J Compos Mater 48:385–405
4. Misra RDK, Yuan Q, Venkatsurya PKC (2012) Mechanics of nanoscale surface deformation in polypropylene-clay nanocomposite. Mech Mater 45:103–116
5. Yuan Q, Rajan VG, Misra RDK (2008) Nanoparticle effects during pressure-induced crystallization of polypropylene. Mater Sci Eng B 153:88–95
6. Yuan Q, Misra RDK (2006) Polymer nanocomposites: recent advances and outstanding issues (invited). Mater Sci Technol 22:742
7. Hayashi A, Minami K, Tatsumisago M (2009) High lithium ion conduction of sulfide glassbased solid electrolytes and their application to allsolidstate batteries. J Non-Cryst Solids 355:1919
8. Stephan AM (2006) Review on gel polymer electrolytes for lithium batteries. Eur Polym J 42:21
9. Bousquet CMI, Mu˜noz-Rojasa D, Casteel WJ, Pearlstein RM, GirishKumar G, Pez GP, Palacín MR (2010) Polyfluorinated boron cluster-based salts: a new electrolyte for application in $Li_4Ti_5O_{12}$/$LiMn_2O_4$ rechargeable lithium-ion batteries. J Power Sources 195:1479
10. Wieczorek W, Zalewska A, Raducha D, Florjan'czyk Z, Stevens JRA, Jacobsson FP (1996) Polyether, Poly(N,N-dimethylacrylamide), and $LiClO_4$ composite polymeric electrolytes. Macromolecules 29:143
11. Hega NA, Afifi MA, Atyia HE, Farid AS (2009) AC conductivity and dielectric properties of amorphous Se80Te20−xGexchalcogenide glass film compositions. J Alloys Compd 477:925
12. Psarras GC, Manolakaki E, Tsangaris GM (2003) Dielectric dispersion and ac conductivity in—Iron particles loaded—polymer composites. Compos Part A 34:1187
13. Almond DP, West AR (1983) Mobile ion concentrations in solid electrolytes from an analysis of ac conductivity. Solid State Ionics 9–10:277
14. Sharma AL, Thakur AK (2011) AC conductivity and relaxation behavior in polymer nanocomposite. Ionics 17:135–143

15. Sharma AL, Shukla N, Thakur AK (2008) Studies on structure property relationship in a polymer-clay nanocomposite film based on $(PAN)_8LiClO_4$. J Polymer Sci B Polymer Phys 46:2577–2592
16. Mohapatra SR, Awalendra K, Thakur, Choudhary RNP (2009) Effect of nanoscopic confinement on improvement in ion conduction and stability properties of an intercalated polymer nanocomposite electrolyte for energy storage applications. J Power Sources 191:601–613
17. Shukla N, Thakur AK (2011) Enhancement in electrical and stability properties of amorphous polymer based nanocomposite electrolyte. J Crysta Solids 357:3689–3701
18. Dyre JC (1988) The random freeenergy barrier model for ac conduction in disordered solids. J Appl Phys 64:2456
19. Dygas JR, Faraj BM, Florjan'czyk Z, Krok F, Marzantowicz M, Zygad E, Monikowska O (2003) Solid State Ionics 157:249–256
20. Anantha PS, Hariharan K (2005) Mater Sci Eng B 121:12
21. Jayathilaka PARD, Dissanayake MAKL, Albinsson I, Mellander BE (2003) Dielectric relaxation, ionic conductivity and thermal studies of the gel polymer electrolyte system PAN/EC/PC/LiTFSI. Solid State Ionics 156:179–195
22. Sharma AL, Thakur AK (2013) Plastic separators with improved properties for portable power device applications. Ionics 19:795–809
23. Cole KS, Cole RH (1941) Dispersion and absorption in dielectrics I. Alternating current characteristics. J Chem Phys 9:341–351
24. Stavrakas TD, Vallianatos A, Kershaw S. Bulletin of the geological society of Greece vol. XXXVI, 2004 Proceedings of the 10th international congress, Thessaloniki, April 2004
25. Dutta A, Bharati C, Sinha TP (2008) Dielectric relaxation and ac conductivity study in SrMg1/3Nb2/3O3. Ind J Eng Mat Sci 15:181–186
26. Pittini YY, Daneshvari D, Pittini R, Vaucher S, Rohr L, Leparoux S, Leuenberger H (2008) Cole–Cole plot analysis of dielectric behavior of monoalkyl ethers of polyethylene glycol (CnEm). Eur Polym J 44: 1191–1199
27. Anantha PS, Hariharan K (2005) AC conductivity analysis and dielectric relaxation behaviour of NaNO3–Al2O3 composites. Mater Sci Eng B 121:12–19
28. Natesan B, Karan NK, Rivera MB, Aliev FM, Katiyar RS (2006) Segmental relaxation and ion transport in polymer electrolyte films by dielectric spectroscopy. J Non-Cryst Solids 352:5205–5209
29. Ramesh S, Arof AK (2001) Ionic conduction via correlated barrier hopping mechanism in CMCSA solid biopolymer electrolytes. Sci Eng B85:11–15
30. Sharma AL, Thakur AK (2011) Polymer matrix-clay interaction mediated mechanism of electrical transport in exfoliated and intercalated polymer nanocomposites. J Mat Sci 46:1916–1931
31. Pavlidou S, Papaspyrides CD (2008) A review on polymer-layered silicate nanocomposites. Prog Polym Sci 33(12):1119–1198
32. Fornes TD, Paul DR (2003) Modeling properties of nylon6/clay nanocomposites using composite theories. Polymer 44(17):4993–5013
33. Deshmane C, Yuan Q, Perkins RS, Misra RDK (2007) On striking variation in impact toughness of polyethylene- and polypropylene-clay nanocomposite systems: the effect of clay-polymer interaction. Mater Sci Eng A 458:150
34. Deshmane C, Yuan Q, RDK (2007) High strength-toughness combination of melt intercalated nanoclay reinforced thermoplastic olefins. Mater Sci Eng A 460:277
35. Mudaliar A, Yuan Q, Misra RDK (2006) On surface deformation of melt-intercalated polyethylene-clay nanocomposites during scratching. Polymer Eng Sci 46:1625
36. Yuan Q, Awate S, Misra RDK (2006) On the non-isothermal crystallization behavior of melt-intercalated polyethylene-clay nanocomposites. J Appl Polym Sci 102:3809
37. Yuan Q, Misra RDK (2006) Impact fracture behavior of clay-reinforced polypropylene nanocomposites. Polymer 47:4221
38. Yuan Q, Awate S, Misra RDK (2006) Non-isothermal crystallization behavior of polypropylene-clay nanocomposites. Eur Polym J 42: 1994–2003
39. Tanniru M, Yuan Q, Misra RDK (2006) On significant retention of impact strength in clay-reinforced high density polyethylene nanocomposites. Polymer 47:2133
40. Nathani H, Dasari A, Misra RDK (2004) On the reduced susceptibility to stress whitening behavior of melt intercalated polybutene-clay nanocomposites during tensile straining. Acta Mater 52:3217
41. Dutta P, Biswas S, De SK (2001) Alternating current conductivity and dielectric permittivity of polyaniline doped with β naphthalene sulphonic acid. J Phys Condens Matter 13:9187
42. Cao W, Gerhardt R (1990) Calculation of various relaxation times and conductivity for a single dielectric relaxation process. Solid State Ionics 42:213–221
43. Gerhardt R, Phys J (1994) Impedance and dielectric spectroscopy revisited: distinguishing localized relaxation from longrange conductivity. Chem Solid 55:1491–1506
44. Page 53 chapter 2, Impedance spectroscopy Theory and Experimental and applications Second Edition Edited by Evgenij Barsoukov and J Ross Macdonald, Wiley-Interscience 2005. Hoboken, New Jersey
45. Sharma AL, Thakur AK (2010) Polymer–ion–clay interaction based model for ion conduction in intercalation-type polymer nanocomposite. Ionics 16(4):339–350
46. Bruce PG (1995) Structure and electrochemistry of polymer electrolytes. Electrochim Acta 40(13–14):2077–2085
47. Wieczorek W, Zalewska A, Raducha D, Florjanczyk Z, Stevens JR, Ferry A, Jacobsson P (1996) Polyether, poly(N, N-dimethylacrylamide), and $LiClO_4$ composite polymeric electrolytes. Macromolecules 29(1):143–155
48. Wieczorek W, Lipka P, Zukowska G, Wycislik H (1998) Ionic interactions in polymeric electrolytes based on low molecular weight poly(ethylene glycol)s. J Phys Chem B 102(36):6968–6974
49. Sun XG, Kerr JB (2006) Synthesis and characterization of network single ion conductors based on comb-branched polyepoxide ethers and lithium bis(allylmalonato)borate. Macromolecules 39(1):362–372